THERMAL TRANSPORT MEASUREMENT OF SILICON-GERMANIUM NANOWIRES

A Thesis

by

YUNKI GWAK

Submitted to the Office of Graduate Studies of
Texas A&M University
in partial fulfillment of the requirements for the degree of

MASTER OF SCIENCE

August 2009

Major Subject: Mechanical Engineering

THERMAL TRANSPORT MEASUREMENT OF SILICON-GERMANIUM NANOWIRES

A Thesis

by

YUNKI GWAK

Submitted to the Office of Graduate Studies of
Texas A&M University
in partial fulfillment of the requirements for the degree of

MASTER OF SCIENCE

Approved by:

Chair of Committee,	Choongho Yu
Committee Members,	Ibrahim Karaman
	Yongmei Jin
Head of Department,	Dennis O'Neal

August 2009

Major Subject: Mechanical Engineering

ABSTRACT

Thermal Transport Measurement of Silicon-Germanium Nanowires. (August 2009)

Yunki Gwak, B.S., Korea Military Academy

Chair of Advisory Committee: Dr. Choongho Yu

Thermal properties of one dimensional nanostructures are of interest for thermoelectric energy conversion. Thermoelectric efficiency is related to non dimensional thermoelectric figure of merit, $ZT = S^2\sigma T / k$, where S, σ, k and T are Seebeck coefficient, electrical conductivity, thermal conductivity and the absolute temperature respectively. These physical properties are interdependent. Therefore, making materials with high ZT is a very challenging task. However, nanoscale materials can overcome some of these limitations. When the size of nanomaterials is comparable to wavelength and mean free path of energy carriers, especially phonons, size effect contributes to the thermal conductivity reduction without bringing about major changes in the electrical conductivity and the Seebeck coefficient. Therefore, the figure of merit ZT can be manipulated. For example, the thermal conductivities of several silicon nanowires were more than two orders of magnitude lower than that of bulk silicon values due to the enhanced boundary scattering.

Among the nanoscale semiconductor materials, Silicon-Germanium(SiGe) alloy nanowire is a promising candidate for thermoelectric materials The thermal conductivities of SiGe core-shell nanowires with core diameters of 96nm, 129nm and 177nm were measured using a batch fabricated micro device in a temperature range of 40K-450K. SiGe

nanowires used in the experiment were synthesized via the Vapour-Liquid-Solid (VLS) growth method. The thermal conductivity data was compared with thermal conductivity of Si and Ge nanowires. The data was compared with SiGe alloy thin film, bulk SiGe, Si/Si_xGe_{1-x} superlattice nanowire, $Si/Si_{0.7}Ge_{0.3}$ superlattice thin film and also with the thermal conductivity of $Si_{0.5}Ge_{0.5}$ calculated using the Einstein model. The thermal conductivities of these SiGe alloy nanowires observed in this work are ~20 times lower than Si nanowires, ~10 times lower than Ge nanowires, ~3-4 times lower than Si/Si_xGe_{1-x} superlattice thin film, Si/Si_xGe_{1-x} superlattice nanowire and about 3 time lower than bulk SiGe alloy. The low values of thermal conductivity are majorly due to the effect of alloy scattering, due to increased boundary scattering as a result of nanoscale diameters, and the interface diffuse scattering by core-shell effect. The influence of core-shell effect, alloy scattering and boundary scattering effect in reducing the thermal conductivity of these nanowires opens up opportunities for tuning thermoelectric properties which can pave way to thermoelectric materials with high figures of merit in the future.

DEDICATION

To my wife Young Kyong Jo, my parents, family and best friend Vinay.

ACKNOWLEDGMENTS

I would like to express my gratitude to all those who supported me for completing this thesis. I am deeply indebted to my advisor Dr. Yu. Without his knowledge and assistance, this study would not have been successful. I would like to thank my family members, especially my wife, Young Kyong Jo and my parents for supporting and encouraging me to pursue this degree. I acknowledge the Republic of Korea Army for their financial support for my degree.

TABLE OF CONTENTS

Page

LIST OF FIGURES

Page

Page

LIST OF TABLES

Page

NOMENCLATURE

ZT	Thermoelectric figure of merit
S	Seebeck coefficient
σ	Electrical conductivity
k	Thermal conductivity
T	Absolute temperature
k_{ph}	Phonon thermal conductivity
c	Volumetric heat capacity
v	Group velocity of phonon
l	Mean free path of phonon
R_H	Resistance of heating membrane PRT
R_s	Resistance of sensing membrane PRT
Q_h	Joule heat on heating membrane PRT
Q_l	Joule heat on heating membrane leg
T_h	Temperature on heating membrane
T_0	Environmental temperature
T_s	Temperature on sensing membrane
Q_2	Heat conduction though nanowire
G_l	Thermal conductance of leg
k_l	Thermal conductivity of leg
A_l	Cross section area of leg

L_l	Length of leg
G_n	Thermal conductance of nanowire
G_i	Thermal conductance of intrinsic nanowire
G_c	Contact thermal conductance
k_i	Thermal conductivity of intrinsic nanowire
A_i	Cross sectional area of nanowire
L_i	Length of part of the nanowire between two inner FIB spots
$G_{NE,s}$	Noise equivalent sample thermal conductance
T_{NE}	Noise equivalent temperature
R_{NE}	Noise equivalent resistance
δv	Johnson noise(random variation voltage)
v_{out}	Sinusoidal output voltage
G_{air}	Air conductance
k_{air}	Air conductivity
A_{eq}	Equivalent surface area of the membrane
D	Distance between two membranes
l_{air}	Air mean free path
k_B	Boltzmann's constant
n	Density of air molecule
R	Ideal gas constant
$G_{radiation}$	Radiation thermal conductance

F_v	View factor
q_1	Heat flow through SiGe core
q_2	Heat flow through SiO_2 shell
q_{total}	Total heat flow
k_1	Thermal conductivity of SiGe core
k_2	Thermal conductivity of SiO_2 shell
k_t	Total thermal conductivity of nanowire
A_1	Cross section area of SiGe core
A_2	Cross section area of SiO_2 shell
A_t	Cross section area of core-shell SiGe nanowire
$f(T_{e1})$	Bose-Einstein distribution for phonons
τ_{12}	Phonons transmissivity
r_{12}	Phonon reflectivity
Pt	Platinum
PRT	Platinum Resistance Thermometer
FIB	Focused Ion Beam

CHAPTER I

INTRODUCTION

1.1 Silicon-Germanium nanowires as a thermoelectric material

Thermoelectric research started in nineteen century with Ioffe who proposed that thermoelectric materials could be used for making durable solid state refrigerators with no moving parts.[1] Today, due to increase in energy demand, thermoelectric devices are being used as energy regeneration system.[2] Thermoelectric device is an application of the Seebeck effect which elucidates that a semiconductor generates voltage difference, when subject to a temperature gradient. Charge carriers such as electrons and holes in a semiconductor diffuse under the influence of a temperature gradient.[3]Conversely, when a voltage is applied to a semiconductor, there occurs a temperature gradient across it. The thermoelectric device consists of n-type and p-type semiconductors. As shown in figure 1, when a temperature gradient is applied across the thermoelectric device, holes in p-type and electrons in n-type diffuse to the cold side. By utilizing these physical phenomena, we can directly convert the heat energy to the electricity. When used as a refrigerator, the electrons in n-type and holes in p-type carrying heat are driven by a voltage difference.

This thesis follows the style of Applied Physics Letters.

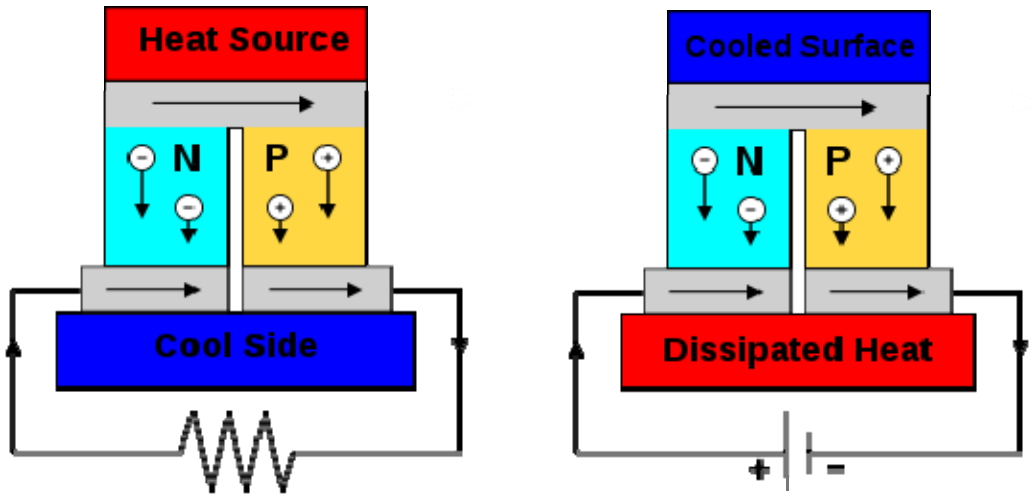

FIG. 1. The Seebeck effect diagram for thermoelectric device.

The efficiency of a thermoelectric device is measured via a non-dimensional thermoelectric figure of merit ZT .

$$ZT = \frac{S^2 \sigma}{k} T \tag{1}$$

where, S is the Seebeck-coefficient, σ is the electrical conductivity, k is the thermal conductivity and T is the absolute temperature. Even though efforts to increase ZT has been going on for 200 years, the efficiency of commercial thermoelectric cooling device have only reached to about 10% of Carnot efficiency and the ZT has remained under 1.[3] In order to substitute the conventional vapor compression refrigerator, with a thermoelectric refrigerator of comparable efficiency, the thermoelectric figure of merit should be over 3. Making high performance thermoelectric materials is challenging because intrinsic properties of material such as S , σ and k are correlated. In general, doping method

for increasing semiconductor's electrical conductivity leads to unexpected thermal conductivity increase due to electrons and a simultaneous decrease of Seebeck coefficient. While lattice imperfections due to alloying and defects can reduce the thermal conductivity because of their ability to effectively scatter phonons. But it also leads electrical conductivity reduction due to scattering of charge carriers.

But recent studies have found that nanoscale materials no longer follow this conventional correlation. Hicks et al. claimed that low dimensional materials can have an enhanced Seebeck coefficient because of different electronic density of state pattern as a result of quantum confinement effect.[4-6] For example, one dimensional nanomaterials such as nanowires and nanotubes shows the sharp edges and peaks in their electronic density of states. In these one dimensional nanomaterials, there occurs a match of the Fermi energy level with electron density of state's peak, which contributes to an increase in the Seebeck coefficient. Moreover, this kind of quantum confinement effect helps to increase the electrical conductivity by enhanced electron mobility.

Nanomaterials have the advantage of being able to decrease thermal conductivity without huge changes of other properties. Thermal conductivity reduction is a critical issue for creating high performance thermoelectric device because lower thermal conductivity could greatly improve the performance of thermoelectric device. Total thermal conductivity of solids is composed of electronic thermal conductivity and phonon thermal conductivity. Phonon thermal conductivity is dominant in semiconductors, while the electronic thermal conductivity is dominant in metals.

Base on the kinetic theory, the phonon thermal conductivity is

$$k_{ph} = \frac{1}{3} cvl \tag{2}$$

where c is the volumetric heat capacity, v is the group velocity of phonons and l is the phonon mean free path. The phonon mean free path is a critical factor to determine the phonon thermal conductivity because at high temperatures, the change of heat capacity and group velocity of phonons is small. Typically phonon mean free path ranges from 1nm to several hundred nanometers. If the diameter of one dimensional nanostructure is comparable to phonon mean free path l, the thermal conductivity of nanowire become lower than that of its bulk counterpart due to the boundary scattering. Thermal transport in one dimensional semiconductor has been studied extensively over the last decade both theoretically and experimentally.[7-10]

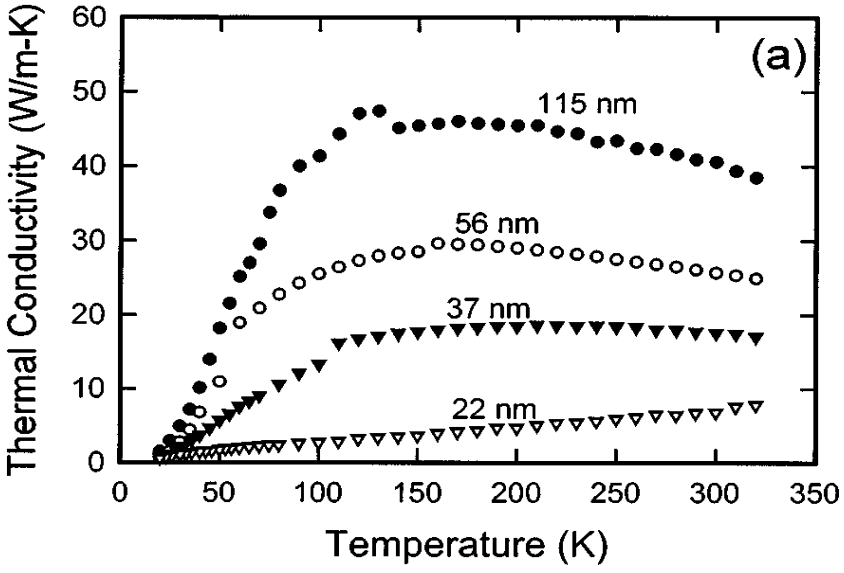

FIG. 2. Thermal conductivity of single crystalline pure silicon nanowires with different diameters[11].

Figure 2 shows experiment results for the thermal conductivity of silicon nanowires with different diameters,[11] It is observed that the measured thermal conductivities of silicon nanowires are two times smaller than that of bulk silicon. Additionally, it clearly shows that the thermal conductivity is dependent on nanowire diameter. As the wire diameter decreases, the corresponding thermal conductivity also decreases. This clearly indicates the influence of phonon-boundary scattering on the thermal conductivity of silicon nanowires. For example, the phonon mean free path of bulk silicon is about 300nm at room temperature. When nanowire diameter becomes comparable to the mean free path, there is boundary scattering and the mean free path gets reduced. Furthermore, rough surface Si nanowires with same Seebeck coefficient have shown about 100 fold decreases in the thermal conductivity as compared to bulk Si, yielding a ZT=0.6.[12] Since Si nanowires have exhibited lower thermal conductivities than their bulk counterparts Recently by varying wire diameter and doping levels of Si nanowires, a $ZT \approx 1$ was obtained even at a low temperature of 200K.[13]

Among thermoelectric semiconductors, SiGe is one of the most important thermoelectric materials because it has shown relatively high thermoelectric efficiency at high temperatures compared to other semiconductors.[14] Thermal conductivity of bulk SiGe alloy is much smaller than that of pure Germanium and the pure Silicon.[15] SiGe based devices are being widely used for spacecraft and space station applications due to their excellent chemical and mechanical stability.[14,16-18]

Work has been already done to find the thermal conductivity of SiGe based materials to make high performance thermoelectric materials. Single crystal n-type bulk $Si_{0.8}Ge_{0.2}$

modeling has shown $ZT \cong 1.3$ at a temperature of 1300K and an optimum carrier concentration.[19] Recently nanostructured p-type and n-type bulk SiGe have shown ZT as high as 0.95 and 1.3 respectively at 900℃.[20,21] SiGe alloy thin films have shown thermal conductivities comparable to bulk SiGe alloy, whereas Si-Ge superlattices have shown lower thermal conductivities compared to bulk SiGe.[22] In Si/SiGe alloy superlattice, the effect of interfacial acoustic impedance mismatch on thermal conductivity has been proposed to be more dominant than in SiGe alloy/ SiGe alloy superlattice, where alloy scattering is the dominant factor than interfacial acoustic impedance to determine thermal conductivity.[23] SiGe nanowires are also expected to give low thermal conductivities. In this work, we report thermal conductivities of SiGe alloy nanowires, which is the first measurement to the best of our knowledge.

1.2 Thermal conductivity measurement for one dimensional nanomaterials

The thermal conductivity of two dimensional thin film and superlattice is measured by using 3ω method. [24-26] This measurement method is insensitive to error from back-body radiation. Black-body radiation is heat radiation from surface of a sample to environment when heat is conducted through the sample. It is especially a critical error for amorphous materials and low thermal conductivity materials. The 3ω method is a utilization of a frequency change depending on temperature. When sinusoidal current source ($i_o \sin(\omega t)$) is applied on the sample, a temperature increase due to Joule heat. Then the electrical resistance R can be modulated at the frequency (2ω) corresponding to temperature change.

The voltage drops through the sample, $v = i_0 \sin(\omega t) R$. It is involving a 3ω component. The thermal conductivity of sample can be converted by using well-defined correlation between $v_{3\omega}$ and the thermal conductivity. This method does not require the accurate steady state of temperature during the measurement. But 3ω method is not suitable for one dimensional nanomaterials such as nanowire and nanotube due to its small size and its dimension. So, the thermal conductivity of SiGe nanowires was measured using batch fabricated micro-device.

CHAPTER II

THERMAL CONDUCTIVITY MEASUREMENT FOR ONE DIMENSIONAL NANOMATERIALS

2.1 Batch-fabricated micro-device for thermal conductivity measurement

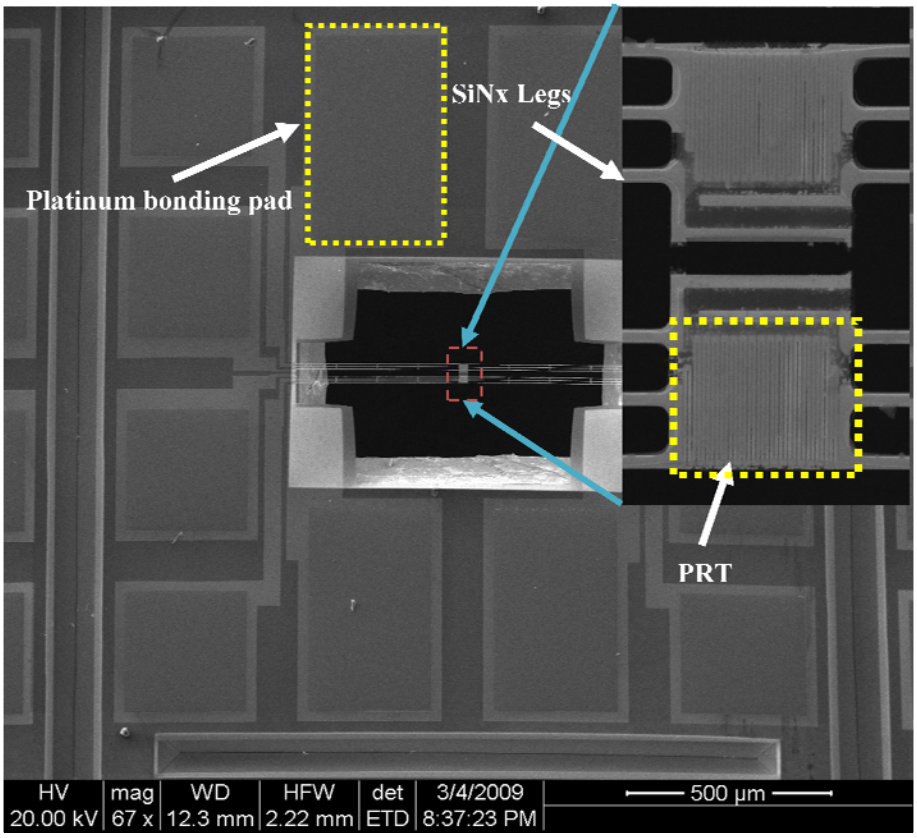

FIG. 3. Scanning electron image of batch fabricated micro-device for thermal conductivity measurement.

Figure 3 shows a scanning electron micrograph image of batch fabricated micro-device which is used for thermal conductivity measurement of one dimensional

nanomaterials. This device has two adjacent suspended $21.5\mu m \times 21.5\mu m$ silicon-nitride(SiN_x) membranes in the middle, separated by a 2μm space for thermal isolation. Each membrane has six 0.5μm thick, $400\mu m$ long and $2\mu m$ wide silicon nitride legs to suspend the membrane and for electrical connection. The platinum resistance thermometer (PRT) coils are patterned in the middle of each membrane. This PRT is intended to measure the temperature of each membrane and also to generate Joule heating by the passage of electricity. Those PRTs are connected to $400\mu m \times 400\mu m$ platinum bonding pads which are used for making electrical connection to the chip-carrier. There is a hole in the middle of the micro-device to facilitate transmission electron microscopy (TEM) analysis. Basically, TEM analysis is done to measure the diameter of SiGe nanowires accurately and to determine crystal structure of the nanowires.

2.2 Sample preparation of SiGe nanowire

The SiGe nanowires were synthesized via the vapor-liquid-solid(VLS) growth mechanism.[27,28] A 1-nm-thick Ni film was thermally evaporated on a hydrogen-terminated n-Si(111) substrate under a base pressure of $1x10^{-6}$ Torr. After ultrasonic cleaning in acetone, samples with size of 1x1 cm^2 were placed into a quartz tube reactor in which a H_2 gas (10% in Ar) was flowed for 30 min at 400 °C so as to remove the oxygen molecules remained inside the tube. The optimal temperature range for nanowire growth was 950–1000 °C, and the ramping rate was ~20 °C/min. During the ramping, ultrathin Ni film was alloyed with

Si to form nanosized $NiSi_x$ agglomerates. These nanosize alloy particles could act as metallic catalyst for the vapor-liquid-solid nanowire growth. For nickel-catalyzed growth of Si_xGe_{1-x} nanowires, source gases, $SiCl_4$ and $GeCl_4$, with a H_2 carrier gas (~10 sccm) were flowed into the reactor from the bubblers containing $SiCl_4$ and $GeCl_4$ liquids. The quartz bubbler was kept at 0 °C. Figure 4 shows a SEM image of SiGe nanowires on silicon substrate.

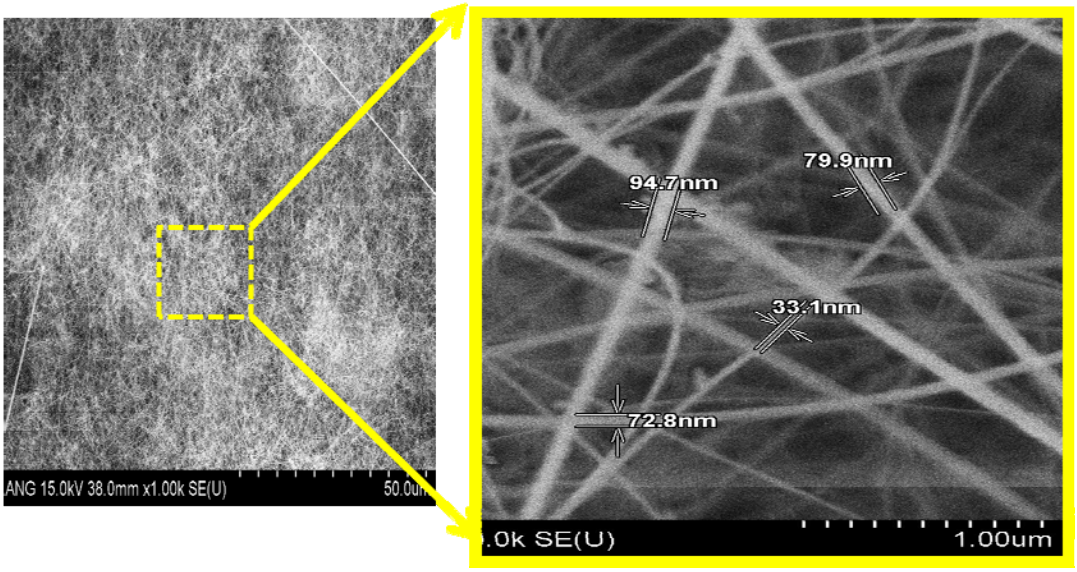

FIG. 4. SEM image of SiGe nanowires on silicon substrate.

Single SiGe nanowire can be placed between the two suspended membranes by using solution drop-dry method.[29] First of all, put the silicon substrate with SiGe nanowires into an empty bottle, then pour Isopropanol as a solvent and after that, ultrasonicate it in order to detach SiGe nanowires from silicon substrate. This step should be done for only tens of seconds, otherwise brittle SiGe nanowires may be damaged by the ultrasound.

Subsequently, one drop of ultrasonicated solution is dropped on the micro-device. Single nanowire often gets bridged between the two membranes after the solution completely dries out.

Figure 5 shows a SiGe nanowire which was successfully bridged between the two membranes.

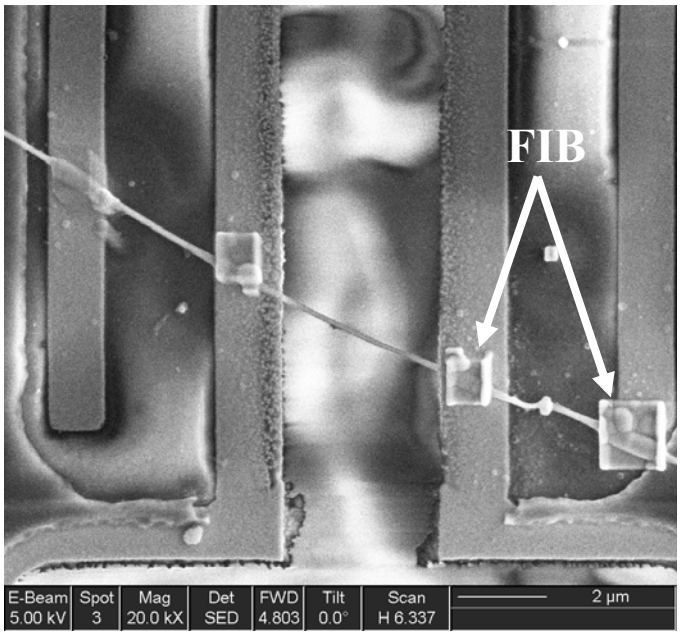

FIG. 5. SEM image of SiGe nanowire which was successfully bridged between the two membranes. Low thermal contact resistance is achieved using FIB(focused ion beam).

The outer native Silicon dioxide layer on SiGe nanowire prevents proper thermal contact between the nanowire and platinum electrode.[30] FIB(Focused Ion beam) is used to rectify this problem. The highly energetic Gallium ion beam of the FIB break through the native oxide layer and allow the platinum to be directly deposited on the exposed core of the nanowire.

Finally the micro-device with SiGe nanowire was placed on a chip-carrier using

silver paint which enables better thermal contact between the micro-device and the chip-carrier. Electrical connection between them is made using Kulicke & Soffa Ltd. 4500 Series Manual Wire/Wedge Bonder. For thermal conductivity measurement, the chip-carrier was placed into a closed cryogenic refrigerator system. (Advanced Research System DE-204).

2.3 Experimental setup

Figure 6 shows a schematic diagram of the experimental setup for thermal conductivity measurement of nanowires. The chip-carrier with micro-device was attached to the cold finger of the cryostat. To minimize conduction and convention due to air, the vacuum level of cryostat was brought below 1×10^{-3}torr. The compressor cools down the cold head by using the Gifford-McMahon refrigeration cycle. The cold head was connected to the compressor though two gas lines. One of the gas lines supplies high pressure helium gas to the cold head, while the other gas line returns low pressure helium gas from the cold head. This pressure difference creates a temperature drop in the cold head. The cold finger should be isolated from the vibrations of the cold head in order to reduce noise, because nanoscale measurements are very sensitive. Helium gas is supplied, which acts as a medium of heat transfer between the cold head and the cold finger. Steady state temperature at the cold finger is achieved by a resistance heater which heats up the cold finger. To obtain temperature information from each membrane, two SR830 lock-in amplifiers were connected to each membrane. In our thermal conductivity measurement, the temperature range of measurement is 40K to 450K.

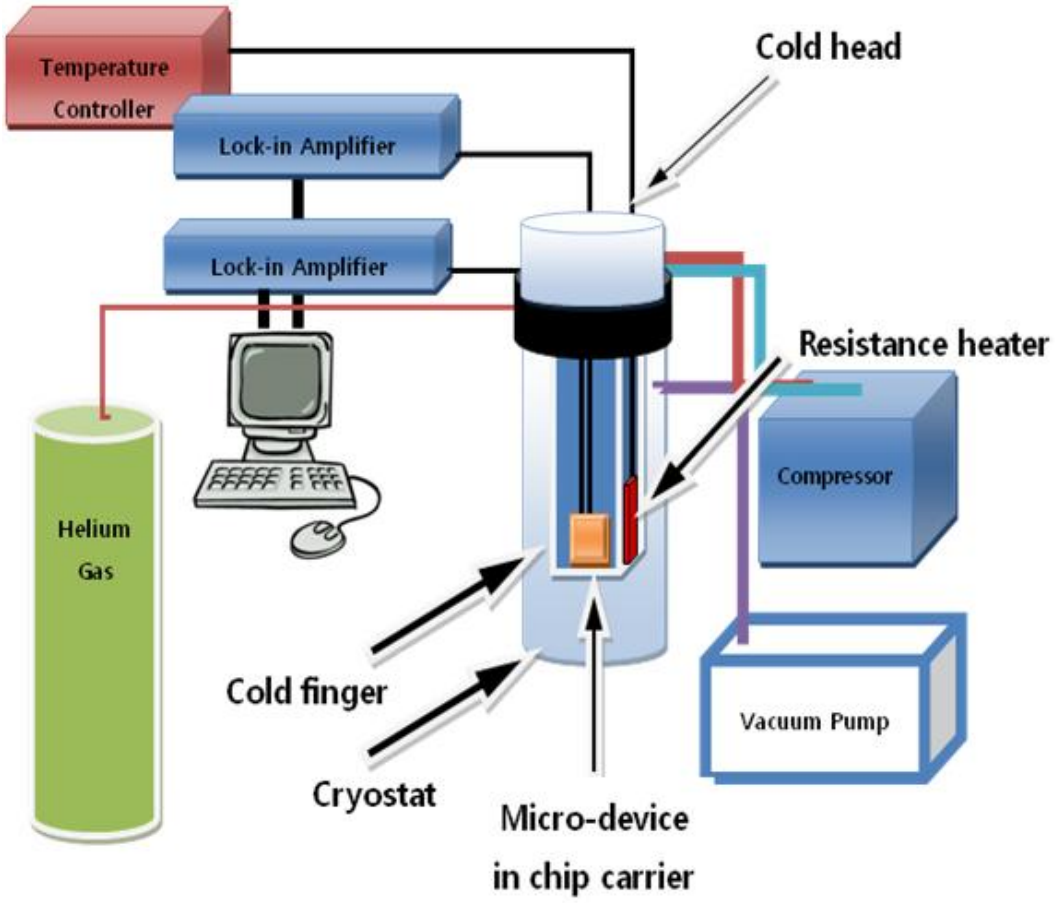

FIG. 6. Schematic diagram of the experimental setup for thermal conductivity measurement of nanowires.

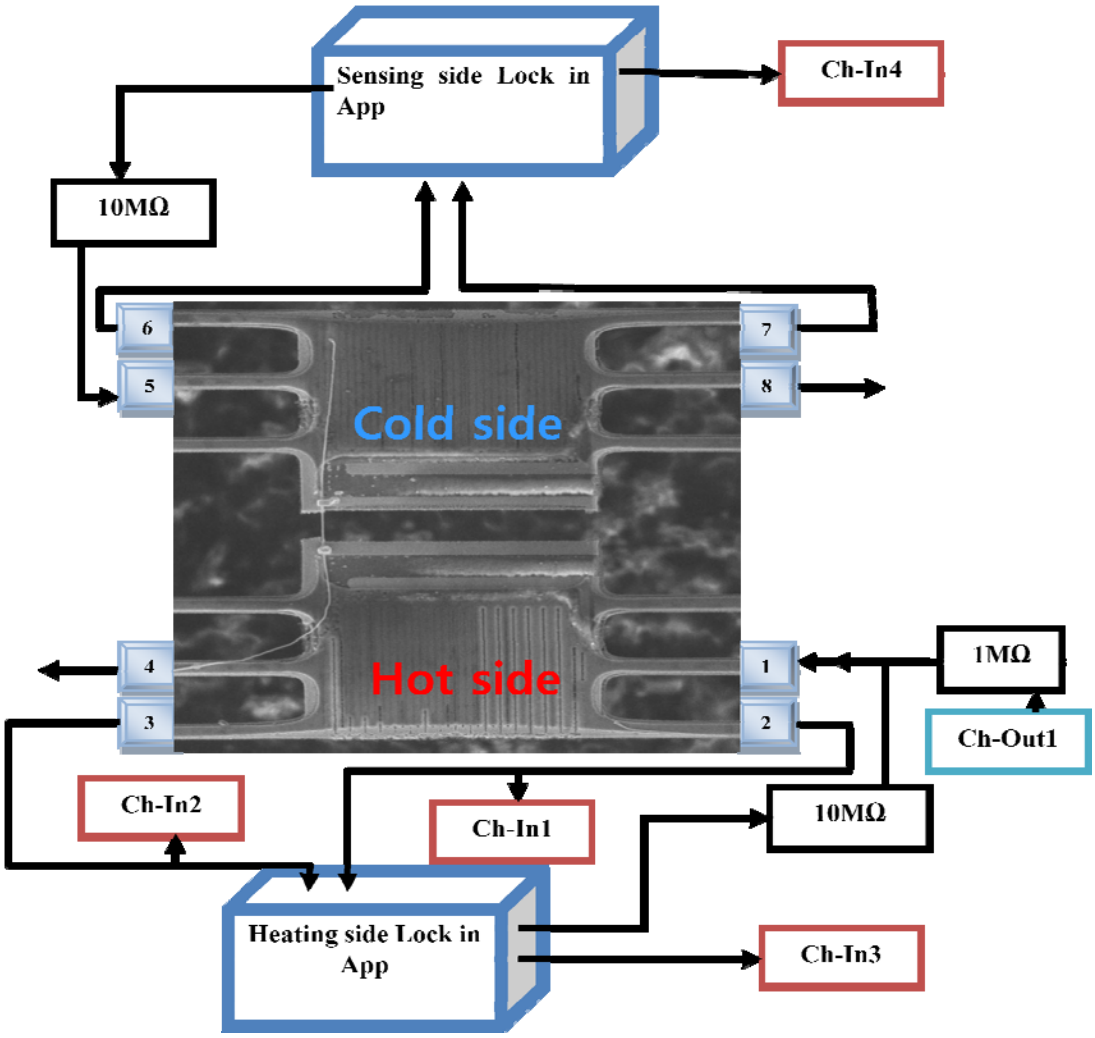

FIG. 7. Schematic diagram showing details of connections between micro-device and measurement instruments.

Figure 7 shows details of connections between micro-device and measurement instruments. DC(Direct Current) was supplied from a DAQ(Data Acquisition) board (Ch-out1→4) for heating PRTs. It gives rise to Joule heating in the heating membrane and some part of this joule heat energy conducts through the nanowire to the other membrane

designated as sensing membrane. Simultaneously, AC(Alternating Current) from lock in amplifier was passed through each PRT line(1→4,5→8) for four probe measurement. Two lock-in amplifiers detect the voltage difference in the PRT line of the heating membrane between terminals 2 and 3 and in the PRT line of the sensing membrane between 6 and 7. The lock-in amplifiers also measure the electric current flowing through the PRT line from 1 to 4 in the heating membrane and the electric current flowing through the PRT line from 5 to 8 in the sensing membrane.

2.4 Thermal conductivity measurement method

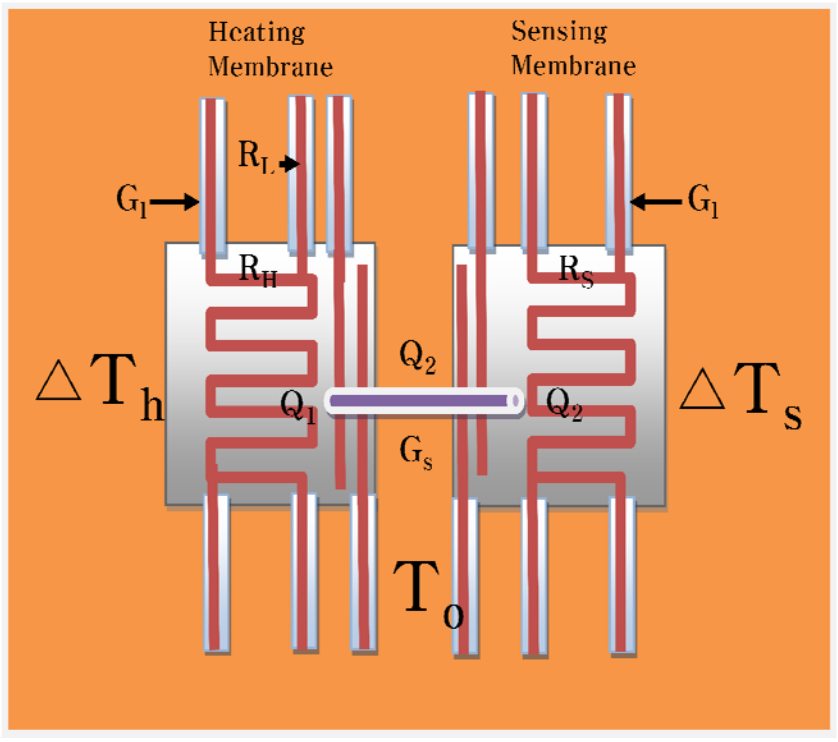

FIG. 8. Schematic diagram of thermal resistance circuit for thermal conductivity measurement.

The heating membrane and the sensing membrane have a PRT with resistance R_H and R_s respectively. The PRT on each membrane is connected to the platinum contact pad through six Pt(Platinum) legs. Four Pt legs of each membrane allow four probe resistance measurement in order to calculate the temperature while the other two Pt legs are intended to measure the electrical conductivity. Each Pt leg's resistance is R_L which is about half of R_H. When DC current flows through the PRT, a Joule heat $Q_h = I^2 R_H$ is generated in the heating membrane. At the same time, a combined heat of $2Q_l = 2I^2 R_L$ is generated in the two Pt legs which supply DC current to the heating PRT. This joule heat energy raises the temperature of the heating membrane to a uniform value of T_h. The chip carrier is at an environmental temperature of T_0. The long narrow legs transfer heat between the chip carrier and the membranes which have low thermal resistance. So, initially before Joule heating, the heating membrane and the sensing membrane are at a uniform temperature T_0 . Therefore, the temperature excursion on heating membrane should be $\Delta T_h = T_h - T_0$. A small amount of the heat, Q_2 conducted through the nanowire from the heating membrane to the sensing membrane contributes to temperature rise, T_s on the sensing membrane. Then the temperature excursion on the sensing membrane is $\Delta T_s = T_s - T_0$. After the heat conduction through the nanowire, the residual heat energy on heating membrane will be $Q_1 = Q_h + 2Q_l - Q_2$. The air conduction and radiation from the two

membranes are negligible since the experiment is done at high vacuum and also because the temperature excursion ΔT_h is small as compared to Q_2. This is discussed in section 2.6 – 'Errors in thermal conductivity measurement'. Heat conduction to the environment takes place through the twelve legs supporting the two membranes. The residual Q_1 is conducted to the environment through the six legs on the heating membrane while Q_2 is eventually conducted to environment through the six legs supporting the sensing membrane. These twelve legs are initially designed to be identical. Thus the total thermal conductance of the six legs on each membrane can be simplified as $G_l = 6k_l A_l / L_l$, where k_l is the thermal conductivity of leg, A_l is the cross sectional area of leg and L_l is the length of leg.

Q_2 can be derived from the thermal resistance circuit shown in figure 8.

$$Q_2 = G_l(T_s - T_0) = G_n(T_h - T_s) \tag{3}$$

where G_n is the thermal conductance of the nanowire, which consists of the intrinsic thermal resistance of nanowire and the thermal contact resistances between nanowire and Pt contact pads on each membrane.

$$G_n = \frac{1}{R_n} = \left(\frac{1}{G_i} + \frac{1}{G_c}\right)^{-1} \tag{4}$$

where $G_i = k_i A_i / L_i$ is the intrinsic thermal conductance of the nanowire, k_i, A_i and L_i are thermal conductivity, cross-sectional area of nanowire and length of part of the nanowire between two inner FIB spots respectively. G_c is the contact thermal conductance

between nanowire and Pt contact pads on each membrane. When temperature excursion ΔT_h on heating membrane is very small, G_i and G_c can be assumed to be constant.

The heat conduction through the twelve legs is one dimensional. Temperature distributions of the twelve legs are solved as follows. When DC voltage is applied to the heating membrane, uniform Joule heat Q_l is generated in each of the two legs. These two legs show a parabolic temperature distribution because the joule heating is proportional to current square. While the other ten legs devoid of Joule heating show a linear temperature distribution. Hence the heat conduction to the environment through the two Joule-heated legs can be represented as $Q_{h,2} = 2(\frac{G_l}{6}\Delta T_h + \frac{Q_l}{2})$, while heat conduction through the other legs on the heating membrane can be given by $Q_{h,4} = 4\frac{G_l}{6}\Delta T_h$ .The heat conduction to the environment through the six legs on the sensing membrane can be given by $Q_{s,6} = 6\frac{G_l}{6}\Delta T_s$. Therefore, the energy conservation equation for micro-device is

$$Q_{h,2} + Q_{h,4} + Q_{s,6} = Q_h + 2Q_l \tag{5}$$

Finally we can derive G_l and G_n as a function of ΔT_h , ΔT_s , Q_h and Q_l

$$G_l = \frac{Q_h + Q_l}{(\Delta T_h + \Delta T_s)} \tag{6}$$

And from Eq. (3)

$$G_n = G_l \frac{\Delta T_s}{\Delta T_h - \Delta T_s} \tag{7}$$

here Q_h and Q_l can be calculated from the DC current and voltage drops across the heating PRT and Pt legs.

The temperature of each membrane can be obtained by converting the measured resistance of each PRT into corresponding temperature by using TCR(Temperature Coefficient of Resistance) = ((dR/dT)/R) of Pt. The resistance versus temperature plot for Pt is shown in figure 9. Pt has the advantage of having a linear resistance temperature relationship over a wide temperature range. The electrical resistance R_s on the sensing membrane is measured using an SR830 lock-in amplifier with a 199 Hz sinusoidal excitation current. The temperature rise of sensing membrane is dependent on DC current I of the heating PRT.

$$\Delta T_s(I) = \frac{\Delta R_s(I)}{\frac{dR_s(I=0)}{dT}}; \quad \Delta R_s(I) = R_s(I) - R_s(I=0) \tag{8}$$

In order to measure temperature rise on the heating membrane, sinusoidal current i_{ac} with frequency 255Hz was coupled to the much larger DC heating current I. An SR830 lock-in amplifier is used to catch the first harmonic component (V_{ac}) of the voltage drop across the heating PRT, which yields a resistance $R_H = v_{ac} / i_{ac}$. This resistance is used to calculate the temperature rise in the heating membrane. The temperature excursion on heating membrane is given by

$$\Delta T_h(I) = \frac{\Delta R_H(I)}{\frac{dR_H(I=0)}{dT}} \tag{9}$$

2.5 Sensitivity of thermal conductivity measurement

The sensitivity of thermal conductivity measurement is closely related to the minimum or noise-equivalent of sample thermal conductance. The noise equivalent sample thermal conductance can be found from the noise equivalent temperature rise. From Eq. (7), we can derive the noise equivalent sample thermal conductance as

$$G_{NE,n} \approx G_l \frac{T_{NE}}{\Delta T_h - \Delta T_s} \tag{10}$$

T_{NE} is closely related with the noise equivalent resistance R_{NE} in the sensing membrane measurement.

$$T_{NE} = \frac{R_{NE} / R_s}{TCR} \tag{11}$$

When lock-in amplifier is used to measure the resistance,

$$\frac{R_{NE}}{R_s} = \frac{\delta v}{v} + \frac{\delta i}{i} \tag{12}$$

where δv and δi are the noise in the AC voltage measurement and noise in the current source associated with that voltage, respectively. At room temperature, δv is determined by the Johnson noise. This is random variation voltage caused due to thermal agitation of charge carriers in a resistor. $\delta v = \sqrt{4k_B T R_s \Delta f} \approx 4.3(nV)$ for a noise bandwidth of $\Delta f \approx 0.3Hz$ which is the typical frequency fluctuation of lock-in amplifier. Typically the voltage sensitivity of our measurement is set as $v = 5 \times 10^{-3}$ V.

Therefore, $\frac{\delta v}{v} = \frac{4.3 \times 10^{-9}}{5 \times 10^{-3}} = 8.6 \times 10^{-7}$

The current from the source is given by $i = v_{out} / R$, where v_{out} is a sinusoidal

199Hz output voltage form the lock-in amplifier . R is a $10.577(M\Omega)$, 25ppm/K precision resistor that is coupled to the sinusoidal voltage output of the lock-in amplifier. This AC output voltage is automatically converted to a constant AC current source by using Labview program.

Therefore,

$$\frac{\delta i_{ac}}{i_{ac}} = \frac{\delta v_{out}}{v_{out}} + \frac{\delta R}{R} \tag{13}$$

The noise level from AC voltage output of lock-in amplifier $(\delta v_{out} / v_{out})$ is about 4×10^{-5}. The resistance fluctuation $\delta R / R$ of the $10.577 M\Omega$ precision resistance is about 2×10^{-6} for a 0.2K fluctuation of room temperature. So, $\delta i_{ac} / i_{ac} \approx 4.2 \times 10^{-5}$. Therefore, noise in the current source is dominant. So, we can estimate $R_{NE} / R_s \approx 4.2 \times 10^{-5}$

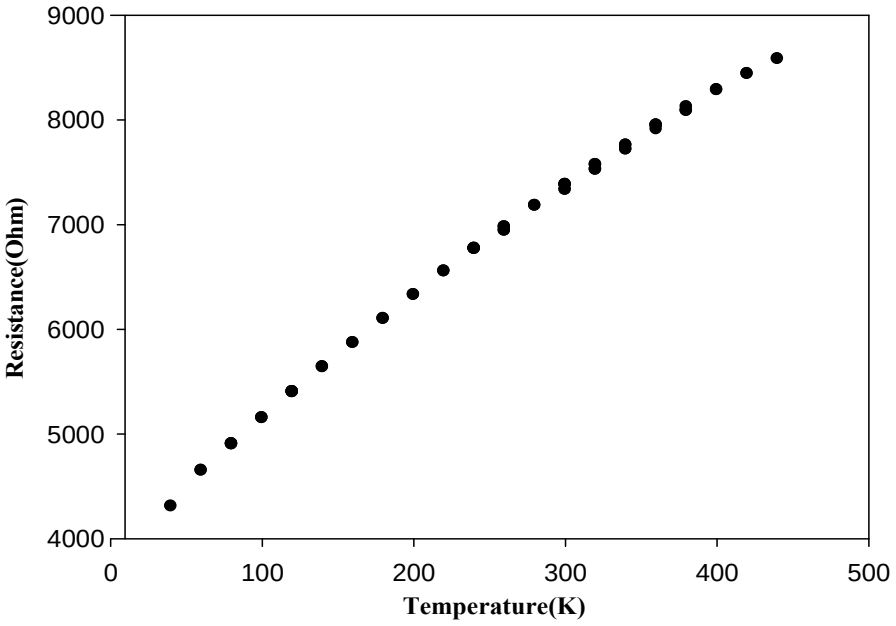

FIG. 9. The resistance(Rs(I=0)) of the PRT as a function of temperature.

Figure 9 shows R_s (I=0) as a function temperature measured from 40K to 450K. It shows almost a linear relationship for the entire range of temperature. The average value of TCR measured for the PRTs is about $1.3\times10^{-3}(1/K)$. In general, TCR for Pt is of the order of $3.7\times10^{-3}(1/K)$. The difference can be attributed to the deposition conditions during micro-fabrication of the micro-device.

From Eq. (11), the noise equivalent of temperature is approximately $T_{NE}\approx 32mK$. The thermal conductance of six legs, G_l is about 87.167×10^{-9} (W/mK). Thus, from Eq. (10), the sample noise equivalent thermal conductance, $G_{NE,n}$ at 300K is 5.5623×10^{-10} W/K for the temperature excursion $\Delta T_h-\Delta T_s=5K$ shown in figure 10.

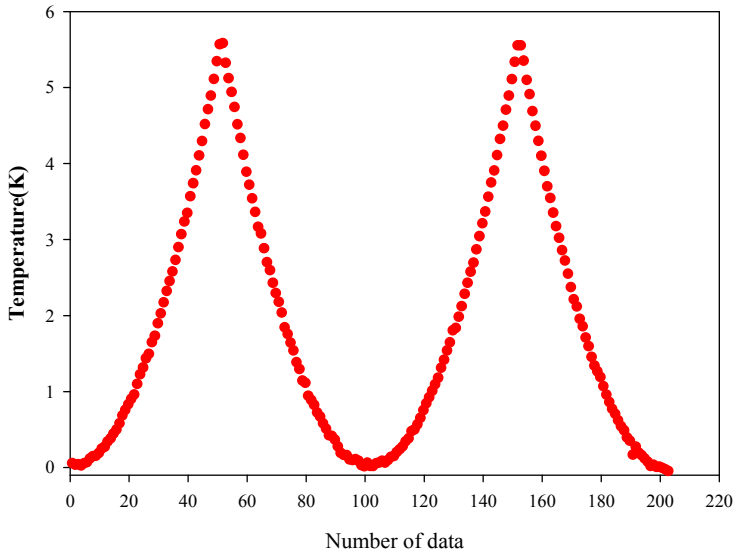

(a) Temperature variation of heating membrane at 300K

FIG. 10. Temperature variation on each membrane for SiGe nanowire 3 at 300K.

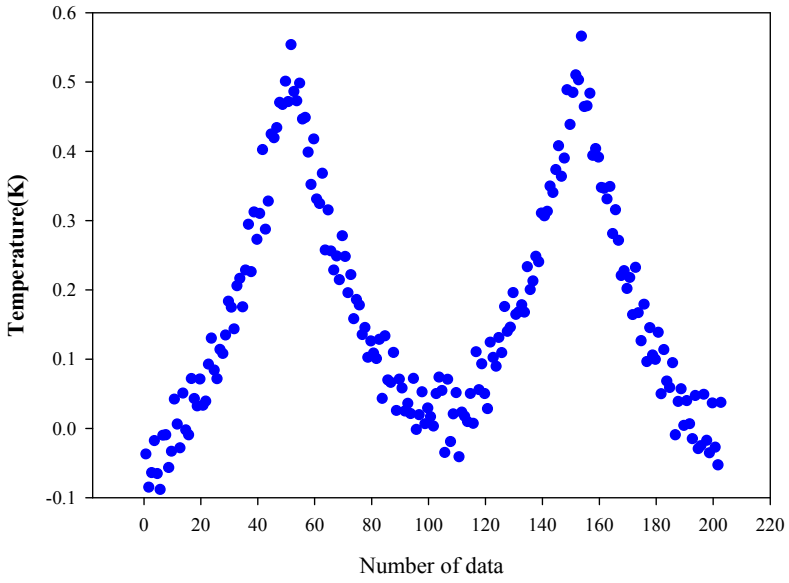

(b) Temperature variation of sensing membrane at 300K

FIG. 10. Continued

2.6 Errors in thermal conductivity measurement

One of the measurement errors occurs by air conduction and membrane radiation in cryostat system. The air conductance can be written as $G_{air} = k_{air} A_{eq} / D$, where k_{air} is the thermal conductivity of air molecules in the cryostat, A_{eq} is equivalent surface area of the membrane and D is the distance between two membranes respectively. According to the kinetic theory, thermal conductivity of air is

$$k_{air} = \frac{Cvl}{3} \tag{14}$$

where C , v , l_{air} are the volumetric heat capacity, average velocity of air molecules and

the mean free path of air molecule respectively.

The mean free path of an air molecule can be written as

$$l_{air} = \frac{1}{\pi d^2 n} \tag{15}$$

where d is average diameter of air molecule and n is the number of molecules per unit volume. Typically diameter of air molecule is roughly $4 \times 10^{-10} m$. From ideal gas equation,

$$PV = Nk_B T, \quad n = \frac{P}{k_B T}, \quad \left(n = \frac{N}{V} \right) \tag{16}$$

where P is the pressure, V is the volume, k_B is the Boltzmann's constant and T is absolute temperature respectively. The vacuum level of the cryostat system used is $10^{-3} torr = 0.1333$(Pa). Therefore, the mean free path of air molecule in the cryostat at room temperature is approximately 6.179cm, which is much larger than distance between two membranes. When the air conduction is overestimated, air conduction is

$$G_{air} = \frac{CvA_{eq}}{3} \tag{17}$$

Normally the volumetric heat capacity of air molecules at room temperature in high vacuum condition is approximately 1.566×10^{-6} $(kJ / m^3 \cdot K)$. The average velocity of air molecules can be derived based on Maxwell-Boltzmann distribution. It is

$$v = \sqrt{\frac{8k_B T}{\pi m}} \tag{18}$$

$$PV = \frac{m}{M} RT = Nk_B T \tag{18.1}$$

$$v = \sqrt{\frac{8RT}{\pi M}} \tag{18.2}$$

where k_B is the Boltzmann's constant, T is the absolute temperature, m is the mass of air

molecule and R is ideal gas constant. The molecular weight of air is roughly estimated as 0.029(kg/mole). So, the average velocity of gas molecule becomes 467.99(m/s). Therefore, the thermal conductivity of air in the cryostat at room temperature is approximately $4.887\times10^{-10}(W/mK)$ from E.q. (14) and air conduction is about $1.129\times10^{-13}(W/K)$ from E.q. (17). It is much lower than the measurement sensitivity, $5.547\times10^{-10}(W/K)$.

Another source of the measurement error could be radiation from the membrane. The radiation thermal conductance can be estimated by using the following equation.

$$G_{radiation}=\sigma(T_h+T_s)(T_s^2+T_h^2)F_vA \tag{19}$$

where F_v and A are the view factor between the two adjacent membrane and the effective radiation surface area of one membrane . It can be shown that $F_vA\approx12\mu m^2$. Thus the radiation heat conductance is $G_{radiation}=7\times10^{-11}(W/K)$ at T=300K. This value is also below the measurement sensitivity. Therefore the error caused due to air conduction and radiation can be ignored.

A major error source in the measurement could be the thermal contact resistance. $R_c=G_c^{-1}$. As discussed in the previous chapter, one of options to decrease thermal contact resistance is FIB which deposits metal on junction between nanowire and Pt contact pad. However, when the nanowire diameter is small enough, FIB is not needed. The total thermal conductance of the sample is $G_n=(G_c^{-1}+G_i^{-1})^{-1}$. If the diameter of nanowire is small enough, intrinsic thermal conductance, G_i become dominant. This is because the

contact area between nanowire and contact pad is proportional to the diameter of the nanowire, while the thermal conductance of intrinsic nanowire is proportional to the square of its diameter.

CHAPTER III

THERMAL CONDUCTIVITY OF SILICON-GERMANIUM ALLOY NANOWIRES

3.1 Result of experiment and discussion

After the thermal conductivity measurement, the SiGe nanowire was taken out from the cryostat system for TEM(Transmission Electron Microscope) analysis. This TEM analysis is done to measure the diameter of SiGe nanowires accurately and to determine crystal structure of the nanowires.

Figure 11 shows TEM images of SiGe alloy nanowires that were measured.

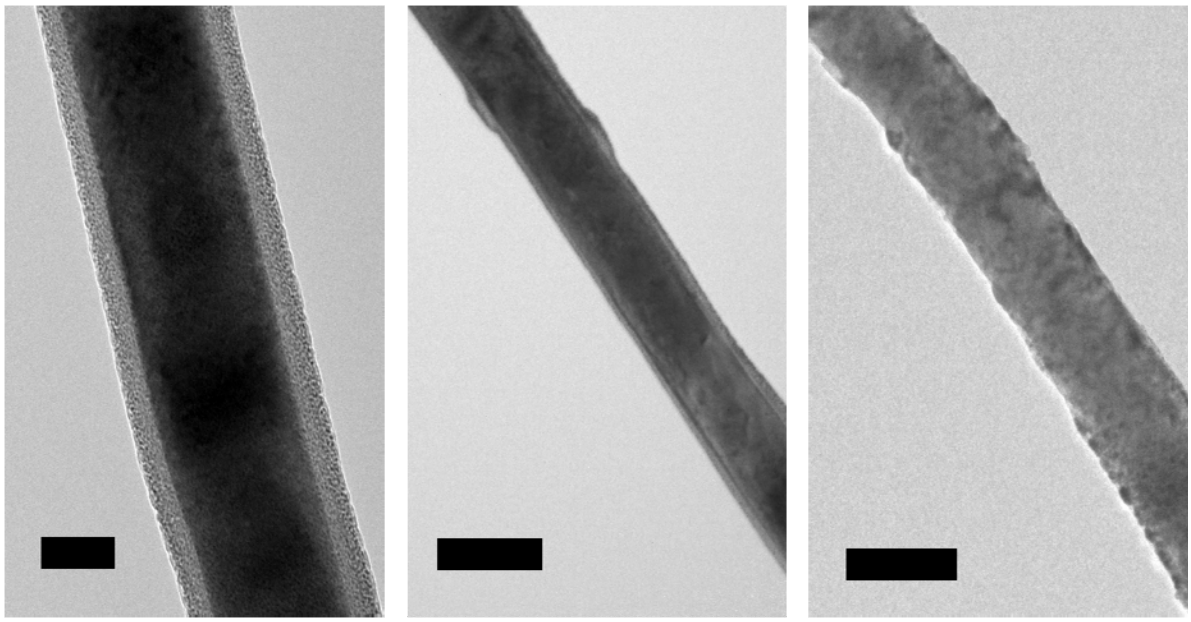

FIG. 11. (a) TEM image of 132nm $Si_{0.44}Ge_{0.56}$ core-shell nanowire with 18nm SiO_2 shell, (b) 133nm $Si_{0.43}Ge_{0.57}$ core-shell nanowire with 12nm SiO_2 shell and (c) 181nm $Si_{0.51}Ge_{0.49}$ core-shell nanowire with 2nm SiO_2 shell. First scale bar is 50nm and others are 200nm each.

Table. 1. gives details about the length, diameter, area and silicon dioxide layer thickness of measured SiGe nanowires. The dimensions of nanowires were measured using a SEM(Scanning Electron Microscope) and a TEM. Note that SiGe NW1 and SiGe NW2 have very thick Silicon dioxide shells, but SiGe NW3 has a very thin SiO_2 shell.

Table. 1. Length, diameter, area and SiO_2 layer thickness of the SiGe nanowires.

	Length(SEM) (μm)	**Diameter(TEM) (nm)**	**Cross-sectional Area (nm^2)**	**SiO_2 layer thickness(TEM) (nm)**
SiGe NW1	4.000	132	13684.78	18
SiGe NW2	3.334	133	13892.90	12
SiGe NW3	4.260	181	25730.43	2

The atomic ratios of Si and Ge were obtained using the energy dispersive spectroscopy(EDS) analysis, which is listed in Table. 2. The EDS analysis was done three times and an average value was taken. The atomic ratio for SiGe NW1 is 44.06% silicon and 55.94% germanium and for SiGe NW2, it is 42.82% silicon and 57.18% germanium. But this EDS analysis has a small error for the atomic ratio of Si to Ge in SiGe core nanowire part, because the electron beam used for the EDS analysis penetrates not only a portion of SiGe core but also a portion of the SiO_2 shell. The real silicon concentration for core SiGe NW1 and SiGe NW2 should be different from the EDS value due to the error introduced by the additional silicon concentration from the SiO2 shell. So the ratio of Si to

Ge in the core parts of NW1 and NW2 are less than 0.44:0.56 and 0.43:0.57 respectively. While the atomic ration for SiGe NW3 is 51.42% silicon and 48.58% germanium and its silicon concentration for core part is not significantly different from the EDS value due to its thin SiO_2 shell. The atomic ratio of Si to Ge in the core part NW3 is almost 1:1.

Table. 2. Atomic ratio of Si and Ge for the nanowries found using EDS system.

	Atomic ratio(%)	
	Silicon	**Germanium**
SiGe NW1	44.06	55.94
SiGe NW2	42.82	57.18
SiGe NW3	51.42	48.58

The high magnification image and diffraction image of SiGe NW1 are shown in figure 12. The diffraction pattern shows an ordered single crystalline core SiGe nanowire, with an amorphous SiO_2 shell. It has a smooth surface and its growth direction was found to be along <220>. SiGe NW2 and SiGe NW3 also exhibit the same pattern of crystal structure, surface roughness and growth direction.

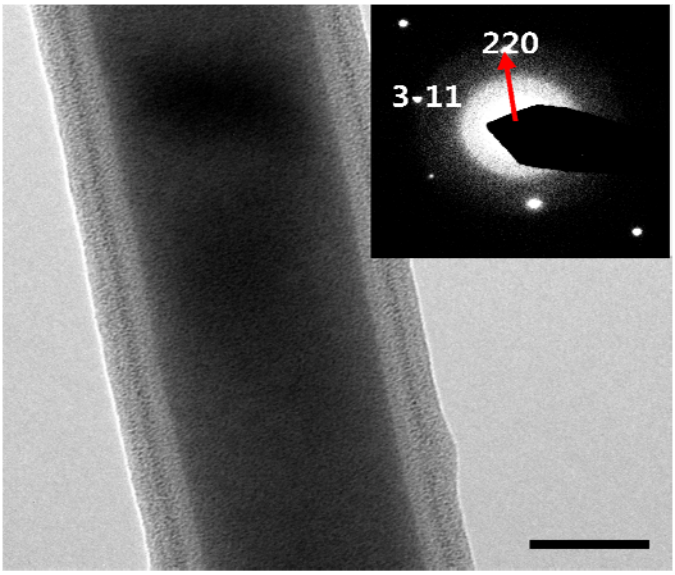

FIG. 12. High magnification image and diffraction pattern of SiGe NW1. Its growth direction is <220> and it is an ordered single crystalline SiGe nanowire, with18nm SiO_2 amorphous shell. Scale bar is 50 nm.

SiGe NW2 was broken at 200K during the thermal conductivity measurement due to electrical static shock shown in figure 13. So thermal conductivity data below 200K is absent.

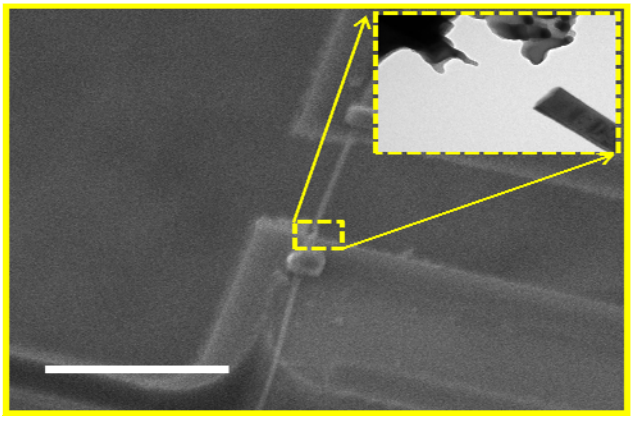

FIG. 13. The broken SiGe NW3 due to electrical static shock. Scale bar is 5μm.

The thermal conductivities of SiGe NW1 core and SiGe NW2 core are calculated by considering core and shell as two parallel thermal resistors.

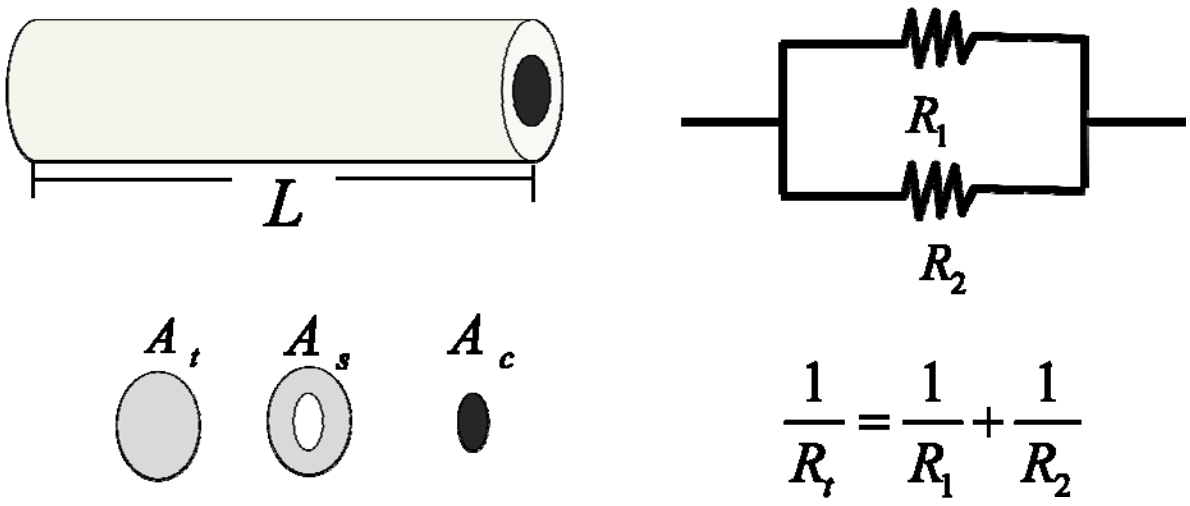

FIG. 14. Schematic representing thermal conductivity calculation for the SiGe nanowire.

If q_1 is the heat flow through the SiGe core and q_2 is the heat flow through the SiO_2 shell, then the total heat flow through the core-shell nanowire is given by $q_{total} = ((k_c A_c + k_s A_s)/L)\Delta T$. Here k_c , k_s , A_c , A_s , L and ΔT are the core thermal conductivity, shell thermal conductivity, core cross-sectional area, shell cross-sectional area, length of the nanowire and the temperature gradient across the nanowire respectively. Thus, the thermal conductivity of core SiGe nanowire is given by

$$k_c = \frac{k_t A_t - k_s A_s}{k_c} \tag{20}$$

where k_t and A_t are the total thermal conductivity and the total cross-sectional area of the

nanowire respectively. The thermal conductivity of shell taken for the calculation, is that of a 0.99μm thick amorphous silicon dioxide layer thermally grown on Si(001).[31] The parallel resistance analogy is not used for the case of SiGe NW3 as the shell thickness in this case is relatively very small. The thermal conductivity is calculated by treating NW3 as a single thermal resistor. Although, when the shell and core are treated as parallel resistors for NW3, the thermal conductivity value differs only by about 3%.

Figure 15 shows the results of experiments for the three core SiGe nanowires with diameters of 96nm, 109nm and 177nm. For reference, experimental data for thermal conductivity of 115nm diameter Si nanowire[11], thermal conductivity simulation result of a 115nm Ge nanowire[32], thermal conductivity of a 30nm period $Si/Si_{0.7}Ge_{0.3}$ superlattice thin film[33]and thermal conductivity of an 83nm diameter single crystalline Si/Si_xGe_{1-x} superlattice nanowire[9] were plotted.

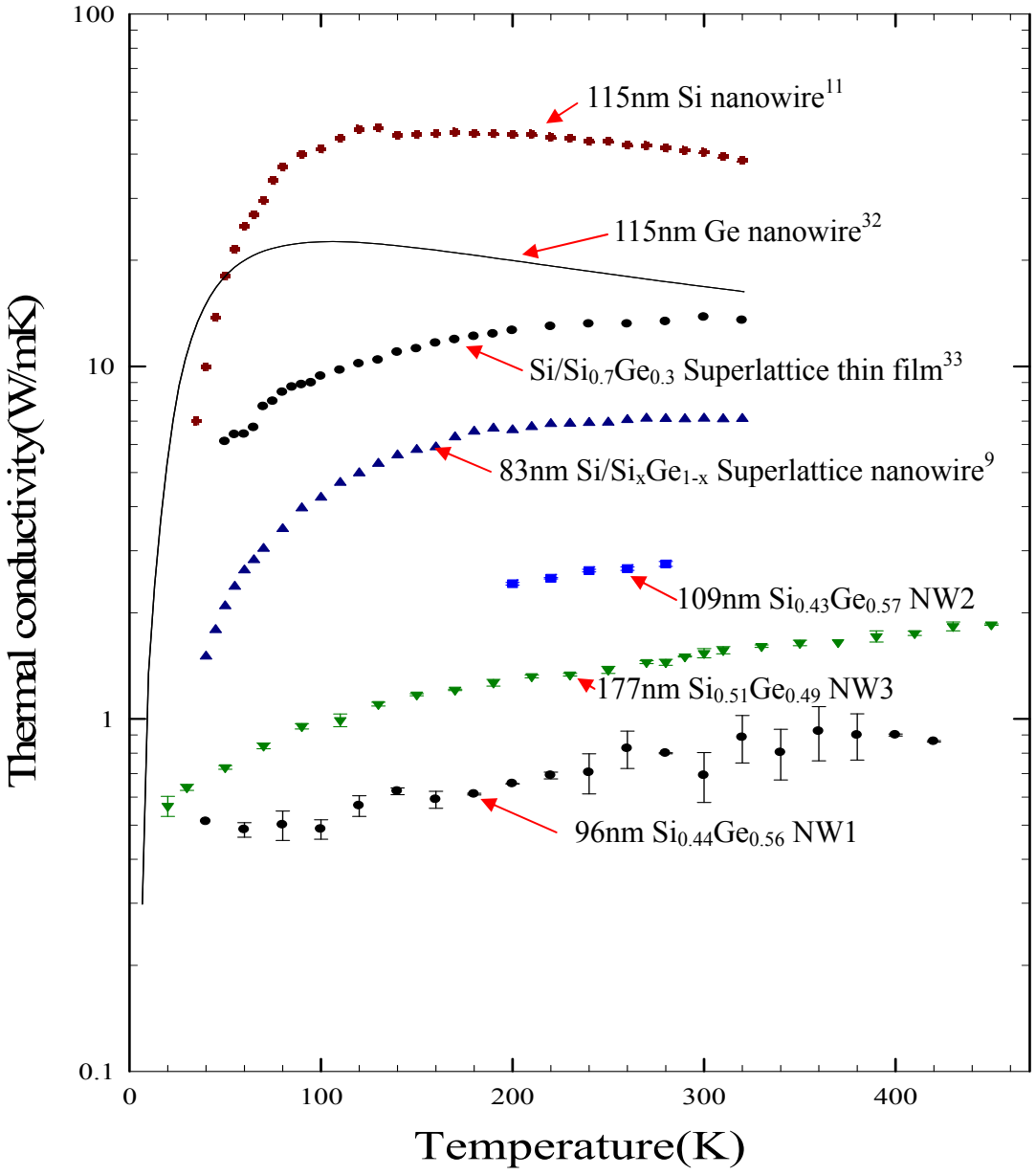

FIG. 15. Experimental thermal conductivity results of the three core SiGe nanowires with core diameters of 96nm, 109nm and 177nm. For reference, experimental data for thermal conductivity of 115nm diameter Si nanowire[11], thermal conductivity simulation result of a 115nm Ge nanowire[33], thermal conductivity of a 30nm period $Si/Si_{0.7}Ge_{0.3}$ superlattice thin film[33]and thermal conductivity of an 83nm diameter single crystalline Si/Si_xGe_{1-x} superlattice nanowire[9] are plotted.

All SiGe NWs have thermal conductivities which are 20 times lower than that of 115nm pure silicon nanowire[11] and 10 times lower than that of pure gemanium nanowire[32]. Alloy scattering is a powerful scattering mechanism and it is a dominant in the SiGe nanowires as compared to Si and Ge nanowires where it is absent. The alloy scattering is the result of atomic mass difference between the Si and Ge and the change of spring constant representing the bonding between atoms in SiGe. This alloy scattering effect smoothens out the peak in the thermal conductivity curve of the SiGe nanowires which is found in Si and Ge at around 100K and 80 K respectively. This is due to the fact that alloy scattering is more dominant than phonon-phonon Umklapp scattering.[9] The phonon-phonon Umklapp scattering sets in at 180K for Si and 101K for Ge.[34] Using linear approximation of the 'Umklapp scattering set-in' temperature, Umklapp scattering is supposed to occur at 140K for the SiGe nanowires. A possible explanation for the shape of the curves is as follows. Before the Umklapp scattering comes into play, that is before 140K the boundary scattering is dominant and the thermal conductivity increases with temperature. After 140K, the phonon frequencies are higher and the dominant alloy scattering comes into play along with the less dominant phonon-phonon Umklapp scattering.[9] But, at higher temperatures, the boundary scattering effect gets relaxed and the balancing act between the increase of alloy scattering and decrease of boundary scattering keeps the curve almost constant at high temperatures.

The thermal conductivity of silicon nanowires shows a strong diameter dependence.[11] But in our study, the thermal conductivity of $Si_{0.51}Ge_{0.49}$ nanowire with diameter of 177nm was lower than that of $Si_{0.43}Ge_{0.57}$ nanowire with 109nm, even though its

diameter is larger. Here $Si_{0.51}Ge_{0.49}$ is almost equal amount of Si and Ge in the alloy, which leads the maximum imperfections and maximum alloy scattering. This phenomena is observed in undoped bulk SiGe as shown by J. P. Dismukes et al.[17] Alloy scattering is more prominent than boundary scattering which depends on diameter. Therefore $Si_{0.51}Ge_{0.49}$ shows lower thermal conductivity than $Si_{0.43}Ge_{0.57}$.

Furthermore, the average thermal conductivity of the SiGe nanowires is 3~4 times lower than that of $Si/Si_{0.7}Ge_{0.3}$ superlattice thin film and the 83nm Si/Si_xGe_{1-x} superlattice nanowire. The superlattice nanowire has shown lower thermal conductivity than the superlattice thin film. It has been suggested that the effect of boundary scattering should be taken into account apart from the effect of alloy scattering and acoustic impedance mismatch to explain this phenomena.[9] SiGe nanowires have alloy scattering which is more dominant than the interfacial phonon scattering. Alloy scattering takes place only the Si_xGe_{1-x} part and not in the Si part of the superlattice nanowire. In the superlattice nanowire whose thermal conductivity is shown in figure 15, x is 0.9 to 0.95. The nanowire samples measured are composed almost entirely of Si_xGe_{1-x} and x is 0.4 to 0.5 which means more powerful alloys scattering is present in these nanowires. Hence, even though the diameter of Si/Si_xGe_{1-x} nanowire is smaller than the diameter of the SiGe nanowire samples measured, the thermal conductivity of SiGe nanowires is lower than that of the Si/Si_xGe_{1-x} superlattice nanowire due to dominance of alloy scattering over other phonon scattering mechanisms.

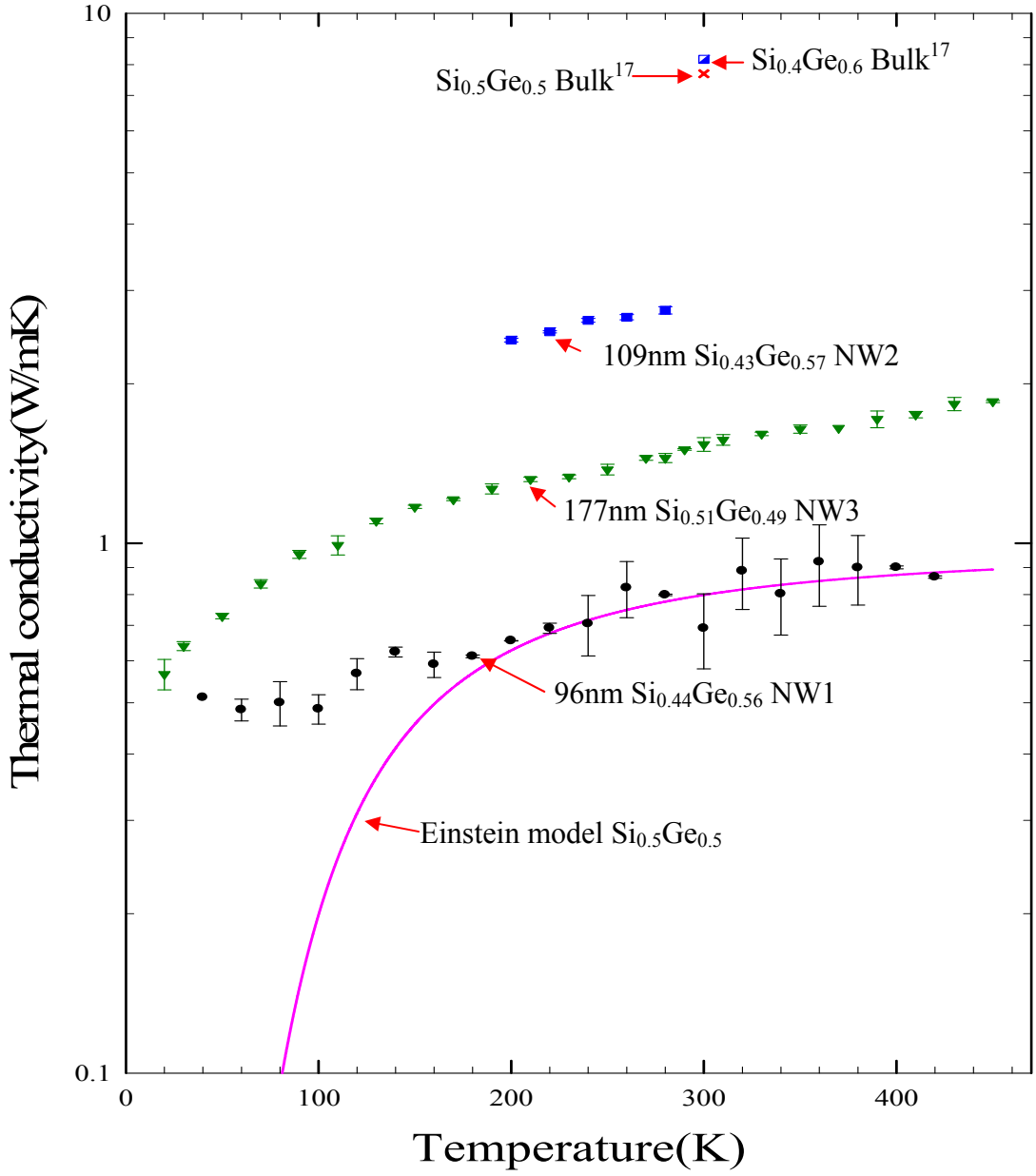

FIG. 16. Experimental thermal conductivity results of the three core SiGe nanowires with core diameters of 96nm, 109nm and 177nm. For reference, experimental data for thermal conductivity of bulk $Si_{0.4}Ge_{0.6}$ and bulk $Si_{0.5}Ge_{0.5}$[17] and minimum thermal conductivity of $Si_{0.5}Ge_{0.5}$ using Einstein thermal conductivity model are also shown.

Although alloy scattering is a major factor, the phonon boundary scattering is also important to explain nanoscale thermal transport, especially at low temperature. The long wavelength phonons at low temperatures are easily scattered by enhanced phonon-boundary scattering and this reduces the thermal conductivity of SiGe nanowires as compared to the thermal conductivity of corresponding bulk SiGe alloy shown in figure 16. Thermal conductivities of all SiGe nanowires measured on an average are ~3 times less than the experimental thermal conductivity data at 300K for $Si_{0.5}Ge_{0.5}$ and $Si_{0.4}Ge_{0.6}$ [17]as shown in figure 16. This can be attributed to enhanced phonon boundary scattering due to the low dimension of the nanowire samples. Moreover, the thermal conductivity of 96nm SiGe NW1 is two times lower than that of 109nm SiGe NW2, which has almost same atomic ratio as the SiGe NW1. This can be partly attributed to the nanowire core diameter difference of SiGe NW1 and SiGe NW2 which leads to different degrees of phonon boundary scattering in the two nanowires. This trend has been observed in Si nanowires which show thermal conductivity reduction with reduction of nanowire diameter due to boundary scattering.[11] Another reason might be the diffuse interface scattering at the SiO_2 shell interface.

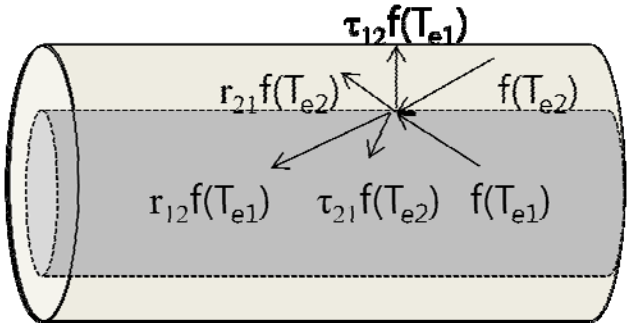

FIG. 17. Transmission and reflection of phonons at an interface[35].

Figure 17 shows diffuse interface scattering at the interface between core and shell. Here T_{e1} represents the temperature of the phonons coming toward the interface and $f(T_{e1})$ is the Bose-Einstein distribution for phonons at T_{e1}. τ_{12} is the phonon transmissitivity from medium 1 into medium 2 and r_{12} is the phonon reflectivity. When heat conduction is perpendicular to an interface, phonons can be reflected or transmitted at the interface. It implies that energy transfer by heat carriers like phonons can be reduced by introducing an interface. The thermal conductivities of SiGe NW1 and SiGe NW2 should be smaller than that of same diameter SiGe nanowire without shell. This diffuse interface scattering of the short wavelength phonons can not only reduce the phonon mean free path but can also destroy the coherence of the phonons.[36]

For the reference, the thermal conductivity of SiGe alloy with 50% Silicon and 50% Germanium was calculated using the Einstein model and is shown by the solid lines in figure 16. The Einstein model assumes the atomic vibrations to be localized damped oscillators instead of waves. Every atom is considered to be a harmonic oscillator with each of them having the same frequency. The thermal conductivity k_E is given by

$$k_E = \frac{{k_B}^2 n^{1/3}}{\pi\hbar}\theta_E \frac{x^2 e^x}{(e^x - 1)^2} \tag{21}$$

$k_B, n, \hbar$, θ_E and x are the Boltzmann constant, number of density oscillators, the reduced Planck's constant times, Einstein temperature and θ_E/T respectively, where T is the temperature.[37] This model gives the minimum thermal conductivity of solids as compared

to the other existing thermal conductivity models. The parameters in the model like the Einstein temperature and the number density of oscillators for Si and Ge were found separately. These parameters were linearly interpolated for $Si_{0.5}Ge_{0.5}$. The thermal conductivity was calculated for Si, Ge and SiGe using the Einstein model.[37-40]

The thermal conductivity of SiGe NW1 is comparable to the minimum possible conductivity as given by the Einstein model. The phonon mean free path can be derived using the Matthiessen's rule.

$$\frac{1}{l_{ph}} = \frac{1}{l_{defect}} + \frac{1}{l_{interface}} + \frac{1}{l_{boundary}} \tag{22}$$

Where l_{defect}, $l_{interface}$ and $l_{boundary}$ are the phonon mean free path of phonon-defect scattering, the mean free path of phonon-interface diffuse scattering and the mean free path of phonon-boundary scattering respectively. As mentioned, for SiGe NW1, these three scattering mechanisms are prevalent and contribute to the very low thermal conductivity.

CHAPTER IV

CONCLUSION

This thesis describes thermal conductivity measurement method for one dimensional nanomaterials and thermal transport characterization of individual SiGe nanowires. Batch-fabricated micro-device was used for thermal conductivity measurement. SiGe nanowires were synthesized based on vapor-liquid-solid mechanism. The diffraction pattern shows an ordered single crystalline core SiGe nanowire, with an amorphous SiO_2 shell. It has a smooth surface and its growth direction was found to be along <220>. The outer native SiO_2 layer on SiGe nanowire prevents proper thermal contact between the nanowire and platinum electrode. So, FIB(Focused Ion beam) is used to rectify this problem. The highly energetic Gallium ion beam of the FIB break through the native oxide layer and allow the platinum to be directly deposited on the exposed core of the nanowire.

Thermal conductivity measurement is carried out using a cryostat system within a temperature range of 40K to 450K. The sensitivity in the thermal conductivity measurement is estimated to be of the order of 10^{-10} W/K at 300 K. Errors due to micro-device radiation and residual air conduction at room temperature are $G_{radiation} = 7 \times 10^{-11} (W/K)$, $G_{air} = 1.129 \times 10^{-13} (W/K)$ respectively. The small error values confirm the reliability of the measurement.

Three different SiGe nanowires with different diameters, different SiO_2 shell thicknesses and different constituent atomic ratios were measured. In order to find the

thermal conductivity of $Si_{1-x}Ge_x$ cores in this study, the core and the shell were considered as two parallel thermal resistors.

SiGe NWs have thermal conductivities which are lower than that of pure silicon and germanium nanowire. Alloy scattering is a powerful scattering mechanism in the SiGe nanowires as compared to the case in Si and Ge nanowires. This alloy scattering is more dominant than phonon-phonon Umklapp scattering and phonon-boundary scattering. Although alloy scattering is a major factor, the phonon boundary scattering is also important to explain nanoscale thermal transport, especially at low temperature. This reduces the thermal conductivity of SiGe nanowires as compared to the thermal conductivity of corresponding bulk SiGe alloy due to enhanced phonon boundary scattering For the reference, The thermal conductivity of SiGe alloy with 50% Silicon and 50% Germanium was calculated using the Einstein model. For the nanowires, alloy, boundary and diffuse interface scattering mechanisms are prevalent and contribute to them having very low thermal conductivities.

These are the first SiGe nanowires thermal conductivity measurements to the best of our knowledge. These experimental data can be used as bases for future thermal conductivity models of semiconductor nanowires. The thermal conductivity values are very low even at low temperatures, thus promising higher thermoelectric figures of merit even at low temperatures. The various thermal conductivity determining effects like the core-shell effect, alloy scattering and boundary scattering can be optimized and tuned to get better thermoelectric materials in the future.

REFERENCES

[1] A. Majumdar, Science **303,** 777-778 (2004).

[2] C. Wood, Reports on Progress in Physics **51,** 459-539 (1988).

[3] F. J. DiSalvo, Science **285,** 703-706 (1999).

[4] L. D. Hicks and M. S. Dresselhaus, Physical Review B **47,** 12727 (1993).

[5] L. D. Hicks and M. S. Dresselhaus, Physical Review B **47,** 16631 (1993).

[6] L. D. Hicks, T. C. Harman, and M. S. Dresselhaus, Applied Physics Letters **63,** 3230-3232 (1993).

[7] R. Prasher, Applied Physics Letters **89,** 063121-3 (2006).

[8] S. G. Walkauskas, D. A. Broido, K. Kempa, and T. L. Reinecke, Journal of Applied Physics **85,** 2579-2582 (1999).

[9] D. Li, Y. Wu, R. Fan, P. Yang, and A. Majumdar, Applied Physics Letters **83,** 3186-3188 (2003).

[10] X. Lu, W. Z. Shen, and J. H. Chu, Journal of Applied Physics **91,** 1542-1552 (2002).

[11] D. Li, Y. Wu, P. Kim, L. Shi, P. Yang, and A. Majumdar, Applied Physics Letters **83,** 2934-2936 (2003).

[12] A. I. Hochbaum, R. Chen, R. D. Delgado, W. Liang, E. C. Garnett, M. Najarian, A. Majumdar, and P. Yang, Nature **451,** 163-167 (2008).

[13] A. I. Boukai, Y. Bunimovich, J. Tahir-Kheli, J.-K. Yu, W. A. Goddard Iii, and J. R. Heath, Nature **451,** 168-171 (2008).

[14] B. Abeles, D. S. Beers, G. D. Cody, and J. P. Dismukes, Physical Review **125,** 44 (1962).

[15] C. J. Glassbrenner and G. A. Slack, Physical Review **134,** A1058 (1964).

[16] B. Abeles, Physical Review **131,** 1906 (1963).

[17] J. P. Dismukes, L. Ekstrom, E. F. Steigmeier, I. Kudman, and D. S. Beers, Journal of Applied Physics **35,** 2899-2907 (1964).

[18] R. J. LaBotz, D. R. Mason, and D. F. O'Kane, Journal of The Electrochemical Society **110,** 127-134 (1963).

[19] C. B. Vining, Journal of Applied Physics **69,** 331-341 (1991).

[20] G. Joshi, H. Lee, Y. Lan, X. Wang, G. Zhu, D. Wang, R. W. Gould, D. C. Cuff, M. Y. Tang, M. S. Dresselhaus, G. Chen, and Z. Ren, Nano Letters **8,** 4670-4674 (2008).

[21] X. W. Wang, H. Lee, Y. C. Lan, G. H. Zhu, G. Joshi, D. Z. Wang, J. Yang, A. J. Muto, M. Y. Tang, J. Klatsky, S. Song, M. S. Dresselhaus, G. Chen, and Z. F. Ren, Applied Physics Letters **93,** 193121-3 (2008).

[22] S. M. Lee, D. G. Cahill, and R. Venkatasubramanian, Applied Physics Letters **70,** 2957-2959 (1997).

[23] S. T. Huxtable, A. R. Abramson, C.-L. Tien, A. Majumdar, C. LaBounty, X. Fan, G. Zeng, J. E. Bowers, A. Shakouri, and E. T. Croke, Applied Physics Letters **80,** 1737-1739 (2002).

[24] G. Chen, C. L. Tien, X. Wu, and J. S. Smith, Journal of Heat Transfer **116,** 325-331 (1994).

[25] T. Yamane, N. Nagai, S.-i. Katayama, and M. Todoki, Journal of Applied Physics **91,** 9772-9776 (2002).

[26] D. G. Cahill, Review of Scientific Instruments **61,** 802-808 (1990).

[27] H. F. Yan, Y. J. Xing, Q. L. Hang, D. P. Yu, Y. P. Wang, J. Xu, Z. H. Xi, and S. Q. Feng, Chemical Physics Letters **323,** 224-228 (2000).

[28] J. W. Dailey, J. Taraci, T. Clement, D. J. Smith, J. Drucker, and S. T. Picraux, Journal of Applied Physics **96,** 7556-7567 (2004).

[29] P. Kim, L. Shi, A. Majumdar, and P. L. McEuen, Physical Review Letters **87,** 215502 (2001).

[30] S. B. Cronin, Y.-M. Lin, O. Rabin, M. R. Black, J. Y. Ying, M. S. Dresselhaus, P. L. Gai, J.-P. Minet, and J.-P. Issi, Nanotechnology **13,** 653-658 (2002).

[31] D. G. Cahill, M. Katiyar, and J. R. Abelson, Physical Review B **50,** 6077 (1994).

[32] N. Mingo, L. Yang, D. Li, and A. Majumdar, Nano Letters **3,** 1713-1716 (2003).

[33] S. Huxtable, Ph.D dissertation, University of California, Berkeley (2002).

[34] M. G. Holland, Physical Review **132,** 2461 (1963).

[35] G. Chen, *Nanoscale Energy Transport and Conversion* (Oxford University Press, Massachusetts, 2005) pp180-185.

[36] R. Yang, G. Chen, and M. S. Dresselhaus, Nano Letters **5,** 1111-1115 (2005).

[37] J. Bodzenta, Chaos, Solitons & Fractals **10,** 2087-2098 (1999).

[38] A. Majumdar. Chang-Lin Tien, F. M. Gerner, *Microscale Energy Transport* (Taylor & Francis, Berkeley California, 1997).

[39] M. Vaccari and P. Fornasini, Journal of Synchrotron Radiation **13,** 321-325 (2006).

[40] J. K. J. John T. Yates, *Molecular Physical Chemistry for Engineers* (University Science Books, Virginia, 2007) pp56-60.

VITA

Yunki Gwak was born in 1982 in Busan, The Republic of Korea. He received a B.S. in Mechanical Engineering from the Korea Military Academy in 2005. He was then commissioned as a Infantry officer. He served in the ROK Army from 2005 to 2007 as a platoon leader and staff officer. He entered the Mechanical Engineering Department at Texas A&M University in 2007 as an M.S. student and graduated in August 2009.

Permanent Address: Department of Mechanical Engineering, 3123, TAMU,
College Station, Texas, 77843-3123, USA.

Chair of Committee: Dr. Choongho Yu

E-mail Address: aido0303@hotmail.com